Research paper

Long non-coding RNA X-inactive specific transcript silencing ameliorates primary graft dysfunction following lung transplantation through microRNA-21-dependent mechanism

Jiwei Li[1], Li Wei[1,*], Zhijun Han, Zhong Chen, Quan Zhang

Department of Thoracic Surgery, Henan Provincial People's Hospital, Zhengzhou University People's Hospital, Henan University People's Hospital, Zhengzhou 450003, PR China

ARTICLE INFO

ABSTRACT

Background: Primary graft dysfunction (PGD) is a known acute lung injury (ALI) and a major cause of fatality post-lung transplantation. Though some long non-coding RNAs (lncRNAs) have been studied in ALI through regulation of microRNAs (miRNAs), their effects on PGD remain undefined. The present study aims to explore the underlying mechanism of lncRNA X-inactive specific transcript (XIST) in PGD after lung transplantation.
Methods: Initially, the expression of miR-21, IL-12A and XIST was determined by RT-qPCR and western blot analysis. The dual luciferase reporter assay, RNA pull-down and RIP assay were performed to identify the targeting relationship between miR-21 and IL-12A and the binding relationship between miR-21 and XIST. Loss- and gain-of-function investigations were conducted in rats treated with prolonged cold ischemia and polymorphonuclear neutrophils (PMNs).
Findings: miR-21 was decreased, whilst XIST and IL-12A were increased in the bronchoalveolar lavage fluid of PGD patients after lung transplantation. Enhanced miR-21 expression in rats and PMNs resulted in downregulated expression of pro-inflammatory factors and chemokines, and enhanced the apoptosis of PMNs. XIST was found to upregulate IL-12A expression in a miR-21-dependent manner. Additionally, XIST silencing enhanced the apoptosis of PMNs and inhibited the neutrophil extracellular trap (NET) formation through upregulation of miR-21 but downregulation of IL-12A *in vivo*.
Interpretation: In summary, lncRNA XIST upregulates IL-12A by binding to miR-21, thereby inducing NET formation and accelerating PGD after lung transplantation. This suggests that inhibition of XIST and NET may be beneficial for the treatment of PGD.

1. Introduction

Primary graft dysfunction (PGD) refers to a severe complication of acute lung injury (ALI) occurring within the initial 3 days after lung transplantation and accompanied by pulmonary edema, hypoxemia, and alveolar infiltrates [1, 2]. Patients suffering from PGD are usually confronted with impaired lung function and higher risk of graft dysfunction, or other complications such as bronchiolitis obliterans syndrome, or chronic allograft rejection [3, 4]. The progression of PGD has been thoroughly investigated with regard to underlying causes such as surgical procedures, the allograft recipient, as well as numerous donor-specific factors [5]. During an acute immune response, neutrophils migrate to the site of inflammation and break down their nuclear contents to form neutrophil extracellular traps (NETs) [6]. Upon the release of NETs, microbes are trapped in NETs to protect dissemination at the infection site [7]. NETs can be pathogenic, and lately, have been demonstrated to be potential regulators in systemic

Research in context

Evidence before this study

Before the study, we used PUBMED retrieval tool with "LncRNA XIST", "miR-21", "IL-12A" and "NET" as keywords, and found that there was no related research from the beginning to the most recent. Prior to this study, there was no study on the functions of "XIST", "miR-21" and "IL-12A" on NET formation in PGD following lung transplantation. Previous studies have only proved that miR-21 is negatively correlated with the pathogenesis of PGD, but its regulatory mechanism and the roles of lncRNAs in PGD have been scarcely understood.

Added value of this study

This study showed that XIST targeted miR-21 to upregulate the expression of IL-12A and induced NET formation to induce PGD after lung transplantation. Targeted inhibition of XIST or activation of miR-21 can be used as a fresh therapeutic maneuver for NET formation in lung transplantation-induced PGD with the advantages of high specificity and outstanding efficacy.

Implications of all the available evidence

Downregulation of XIST could be used as a promising therapeutic intervention to treat NET formation. In the future, XIST or miR-21 may be adopted to develop targeted drugs for PGD, because the formation of NET leads to PGD.

inflammation-related diseases, including sepsis, injury after acute liver ischemia-reperfusion, and transfusion-associated acute lung injury [8]. In the realm of PGD, a previous report demonstrated decrease in NETs alleviates PGD post lung transplantation [9,10], providing a basis of therapeutic targeting of PGD. Given the correlation of PGD progression with poor outcomes, and the paucity in effective treatment modalities to tackle the same [11,12], it is imperative to investigate novel therapeutic targets for PGD.

Long non-coding RNAs (lncRNAs) are a group of functional long RNA transcripts with length greater than 200 nucleotides involved in various biological processes [13,14]. Since their initial discovery, lncRNAs have been revealed to be dysregulated in a variety of human diseases [15]. LncRNA X-inactive specific transcript (XIST) is a newly found lncRNA participating in the initiation and progression of multiple cancers and could serve as a biomarker for cancer treatments, including pancreatic cancer and lung adenocarcinoma [16,17]. Intriguingly, it has been reported that XIST is a competing endogenous RNA (ceRNA) for microRNA-137 (miR-137) to regulate the development of non-small cell lung cancer (NSCLC) [18]. MicroRNAs (miRNAs) are small non-coding RNAs with expression found in various cells and tissues, and widely demonstrated to participate in the progression of multiple human diseases, providing intriguing biological markers for the outcomes of lung transplantation [19,20]. In the context of PGD, miR-21 has been found to negatively correlate with the grade of PGD [21]. Moreover, miR-21$-$5p has been proposed as an interesting biomarker to treat ALI caused by hyperoxia [22]. Besides, miR-21 has been revealed to bind to the 3′untranslated region (3′UTR) of the interleukin (IL)$-$12 [23]. IL-12 consists of two subunits: IL-12A and IL-12B and induces inflammation [24]. It has been revealed that the polymorphism of IL-12A leads to the genetic susceptibility to chronic obstructive pulmonary disease in Chinese people [25]. In addition, IL-23, a member of the IL-12 class, is recognized as an underlying target for the PGD treatment [26]. Based on these findings collectively, this study aims to investigate the regulatory network of XIST/miR-21/IL-12A in PGD, with a hypothesis that

the XIST may regulate IL-12A expression by acting as a ceRNA of miR-21 to affect NET formation and consequently to influence PGD post lung transplantation.

2. Materials and methods

2.1. Ethical statement

This study protocol was approved by the Ethics Committee and Experimental Animal Ethics Committee of Henan Provincial People's Hospital. Written informed consent was obtained from all participants or their relatives. The animal experiment strictly adhered to principles to minimize the use, pain and suffering of the experimental animals.

2.2. Study subjects

A total of 42 patients who received allogeneic lung transplantation at the Henan Provincial People's Hospital from August 2015 to August 2017 were enrolled for the study. Donors from brain death were the source of lungs for transplantation. The patient population consisted of 16 patients with idiopathic pulmonary fibrosis, 9 patients with interstitial lung disease, 6 patients with chronic obstructive pulmonary disease, and 11 patients with sarcoidosis. After lung transplantation, 24 patients suffered from PGD whilst the rest did not, as assessed by the PGD grading scale formulated by the International Society of Heart and Lung Transplantation (ISHLT). There was no significant difference in the age, gender, body mass index, and transplantation type among the patients. The bronchoalveolar lavage (BAL) was performed in the right middle lobe or left lingula, and BAL fluid (BALF) from the enrolled patients was collected [21]. In brief, 50 mL sterile normal saline was quickly instilled into the bronchoalveolar twice with the BALF aspirated manually using a 60 mL syringe. The lavage fluid collected initially was removed, and the lavage fluid collected the second time was filtered and preserved at -80 °C for further analysis. A portion of BALF was centrifuged at 1200 rpm for 10 min at 4 °C. The obtained supernatant was preserved at -80 °C for NETs-DNA analysis and the obtained cells were used for May-Grunwald-Giemsa (MGG) staining (G3100, http://www.solarbio.com) to determine cell population [27].

2.3. Rat model of left single lung transplantation

Left single lung transplantation was conducted based on a previous study [28,29]. A total of 180 Sprague-Dawley (SD) rats aged 8 - 12 weeks and weighing 200 - 250 g were purchased from the Experimental Animal Center of Henan Province (Zhengzhou, Henan, China). The rats were randomly assigned into donors and recipients. The left lungs of the donors were completely immersed in 20 mL preservative fluid at 4 °C for prolonged cold ischemia (PCI) for 18 h prior to transplantation into the recipient. After general anesthesia, a 14 G trachea cannula was inserted into the recipient rats in the overhead position. After that, the recipient lay in a right lateral position, followed by shaving. The left lung was then pulled out and fixed outside the thoracic cavity. Upon the exposure of the mediastinal pleura, the proximal end of the left lung bronchus was clipped using a noninvasive microvascular clamp by adjusting parameters in the rodent ventilator (model R415; RWD Life Science, Shenzhen, CHINA). After that, 100 U/kg heparin was injected into the left atrium through the pulmonary branches at the distal end, followed by clipping of the proximal end of the left pulmonary vein. The donor lung was taken out from the preservative fluid and placed on the original left lung of the recipient to ensure the left pulmonary artery, pulmonary vein and bronchus of the donor and the recipient were anastomosed. After hemostasis, the intrathoracic drain was inserted into the thoracic cavity and connected to an empty syringe to drain the blood and air.

After respiratory and consciousness recovery, the trachea cannula was removed. When the recipient was fully awake, the intrathoracic drain was removed. The donor lungs without PCI were transplanted to the recipients as the sham operation. The recipients were transduced with lentiviral vectors (LV) 24 h and 2 h prior to the model establishment. The successful rate of modeling was 90% (n = 162). The LVs pLVX-Tight-Puro (P0253) and pLKO.1 (SCH002) were purchased from Miaoling Bio. Inc. (Wuhan, Hubei, China) and Sigma-Aldrich Chemical Company (St Louis, MO, USA), respectively. The LVs expressing miR-21 (LV-miR-21), short hairpin RNA (shRNA) targeting XIST (sh-XIST), and miR-21 sponge (inhibiting miR-21 expression) as well as their corresponding controls were constructed by the Miaoling Bio. Inc. (Wuhan, Hubei, China).

2.4. Lung analysis in recipients

The recipient rats were anaesthetized at the 8th h after transplantation using medetomidine (1 mg/kg), midazolam (0.05 mg/kg), and fentanyl (0.02 mg/kg), followed by intubation (300 μL room air/120 strokes/min). A midline abdominal incision was then created, and the thoracic cavity was opened to expose the lung and heart block. The right bronchus and pulmonary vein were clamped for 5 min (75 μL room air; 120 strokes/min) and the blood was collected from the left ventricle to assess the oxygenation function of the transplanted left lobe and the partial pressure of oxygen (pO_2) using an ABL80 FLEX CO—OX blood oximetry analyser (Radiometer, Copenhagen, Denmark). In addition, 200 μL cold phosphate-buffered saline (PBS) was infused into the trachea three times with the right bronchus clamped in order to collect BALF [30]. Subsequently, the upper portion of left lung was excised and weighed before (wet weight) and after (dry weight) drying in an oven at 80 °C for 72 h. The wet weight was divided by dry weight to calculate the wet/dry (W/D) ratio. The lower portion of left lung was fixed with 10% buffered formalin for 24 h, embedded with paraffin, and sliced into sections, followed by hematoxylin and eosin (HE) staining. The pathological changes of the lung tissues were observed under the optical microscope. The lung injury was scored using semi-quantitative method by the pulmonary pathologists according to the following criteria: alveolar hemorrhage, vascular congestion, alveolar fibrin and leukocyte infiltration. Each of these criteria was graded on a 4-level scale of abnormalities and scored from 0 to 3, respectively [31].

2.5. Masson's trichrome stain

The slide was put in Masson's ponceau acid complex solution for 5 min of reaction and washed for 1 min. Then the slide was immersed in 2% glacial acetic acid solution I and II for 1 min, rinsed for 15 min, differentiated in 1% phosphomolybdic acid solution for 5 min and washed under running water for 1 min. Next, the slide was placed in bright green dye solution for 5 min, washed for 1 min, immersed in 2% glacial acetic acid solution I and II for 1 min, and rinsed for 15 min. After dehydration and blocking, the slide was observed under a light microscope and scored by a blind method. According to the previously revealed rating (0−4 points) [32,33], 0 point represents no increase in connective tissue; 1 point represents that the thinner fibers occupy less than 50% of the inflammatory cell infiltration localization, and no thick collagen; 2 points represent that the thinner fibers occupy more than 50% of the inflammatory cell infiltration localization, and no thick collagen; 3 points represent that all the inflammatory cell infiltration localization is filled with the thinner fibers, and the amount of thick collagen is between 10% and 49%; 4 points represent that all the inflammatory cell infiltration localization is filled with thinner fibers, and the amount of thick collagen exceeds 50%. Five high-power visual fields from each section were observed, and the average value was taken as the severity of fibrosis score (F score). The average value of all sections on the same side of one group

was regarded as the fibrosis score of the group. The experiment was run in triplicate.

2.6. Enzyme linked immunosorbent assay (ELISA)

The levels of CC-chemokine ligand 2 (CCL2), interleukin (IL)−6, IL-8, C-X-C motif chemokine 10 (CXCL10) in clinical BALF samples and rats BALF samples were measured using ELISA in strict accordance to the instructions of their respective ELISA kits (Cusabio Biotech Co., Ltd., Wuhan, Hubei, China). The experiment was repeated three times.

2.7. Polymorphonuclear neutrophil (PMN) isolation, culture, and transfection

PMNs were isolated from peripheral blood donated by healthy volunteers. The collected peripheral blood was overlaid on lymphocyte separation medium (LSM), followed by centrifugation of the layered solution at 800 × g at 21 °C for 30 min. The bottom red layer was resuspended in 3% Dextran-PBS solution for 30 min. Afterwards, the supernatant was transferred into a fresh tube and centrifuged to lyse the red blood cells and enrich the PMNs. The enriched PMNs were further sorted using the flow cytometer (Galios; Beckman Coulter, Roissy, France). The PMNs with a purity > 95% were cultured in Roswell Park Memorial Institute 1640 medium (Sigma-Aldrich Chemical Company, St Louis, MO, USA) containing 10% fetal bovine serum (FBS, Thermo Fisher Scientific, Waltham, MA, USA) [34].

The PMNs were seeded into a 24-well plate. When cells were 50% - 60% confluent, the transfection was conducted in accordance with Lipofectamine 2000 protocols (Invitrogen Inc., Carlsbad, CA, USA) for 24 h. miR-21 mimic, miR-21 mimic negative control (NC), miR-21 inhibitor, miR-21 inhibitor NC, scramble sh-NC, shRNA against IL-12A or XIST (sh-IL-12A or sh-XIST), and plasmids overexpressing IL-12A or XIST were all purchased from Guangzhou RiboBio Co., Ltd. (Guangzhou, Guangdong, China).

2.8. Flow cytometry

The PMNs were plated into a 6-well plate, cultured for 1 h, and treated with 10 umol/L phorbol myristate acetate (PMA, Sigma-Aldrich Chemical Company, St Louis, MO, USA) or 50% BALF. After 48 h, the PMNs were transferred into an Eppendorf (EP) tube, detached with trypsin, and washed two times with PBS. The PMNs were incubated at 4 °C avoiding exposure to light for 30 min with the addition of phycoerythrin (PE)-conjugated antibody against active caspase-3 (Becton Dickinson, San Jose, CA, USA) and fluorescein isothiocyanate (FITC)-conjugated monoclonal antibody (mAb) against CD66b (Beckman Coulter, Miami, FL, USA). The PMNs were centrifuged at 878 × g for 5 min to remove the supernatant, and then washed three times with PBS. After resuspension using 300 μL PBS, apoptosis was detected using a flow cytometer (Accuri C6, BD Biosciences, San Jose, CA, USA).

2.9. NET release quantification

The obtained PMNs were seeded into a 24-well plate at a density of 4 × 10^5 cells/well, cultured for 1 h and treated with 10 μmol/L PMA (Sigma-Aldrich Chemical Company, St Louis, MO, USA). The PMNs were treated with equal amount of PBS as control. After 3 h, the PMNs were centrifuged at 4 °C for 5 min at 450 × g, followed by collection of the supernatant without cells. Rabbit polyclonal antibody to neutrophil elastase (NE; 1: 1000, 50 μL/well, ab21595, Abcam, UK) was added into a 96-well microplate (Nunc MaxiSorp, Thermo Scientific, Waltham, MA, USA), and incubated at 4 °C overnight. Afterwards, the PMNs were blocked with 5% bovine serum albumin (BSA). Then BALF (50 μL/well) or supernatant collected from

PMA-treated PMNs was incubated at room temperature for 2 h with horseradish peroxidase (HRP)-conjugated antibody to DNA (1: 100, 50 μL/well, Cell Death Detection ELISA Kit; Roche Applied Science, Indianapolis, IN, USA) and for 30 min with 2, 2′-Azino-Bis-3-ethyl-benzothiazoline-6-sulfonic acid (100 μL/well, Thermo Fisher Scientific Inc., Waltham, MA, USA). The optical density (OD) detected at 405 nm wavelength minus the OD at 490 nm was used as a measure of the relative content of NET-DNA complexes [8].

2.10. Immunofluorescence staining

The lung tissue sections (5 μm) were paraffin-embedded and fixed on the slides. Following deparaffinizing, clearing, and blocking, the sections were incubated with rabbit antibody to citrullinated histone H3 (Cit-H3; 1: 100, ab219407, Abcam, UK) and goat antibody to NE (sc-9520, Santa Cruz Biotechnology, Inc, Santa Cruz, CA, USA) respectively, at 4 °C overnight. The following day, the sections were incubated with secondary antibody, Alexa Fluor 488 goat anti-rabbit antibody to immunoglobulin G (IgG) (1: 200, ab150073, Abcam, UK) and Alexa Fluor 647 goat anti-rabbit antibody to IgG (1: 500, ab150131, Abcam, UK) at room temperature for 1 h. The DNA was stained by 4′,6-diamidino-2-phenylindole (DAPI, Life Technologies, Carlsbad, CA, USA) and the formation of NET was observed under a confocal microscope.

The PMA-treated PMNs were settled in the polylysine-coated slides (Corning Incorporated, Corning, NY, USA) and fixed with 4% polyformaldehyde (Sigma-Aldrich Chemical Company, St Louis, MO, USA) for 30 min. The PMNs were incubated with SYTOX Green (Thermo Fisher Scientific, Waltham, MA, USA) and Hoechst 33,342 (ImmunoChemistry Technologies, Bloomington, MN, USA) for 15 min. After that, the sections were mounted using anti-fluorescence quencher, and NET formation was observed under the confocal microscope.

2.11. Reverse transcription quantitative polymerase chain reaction (RT-qPCR)

The total RNA was extracted from PMNs or rat BALF using the Trizol kit (16,096,020, Thermo Fisher Scientific, Waltham, MA, USA). And then, 5 μg RNA was reversely transcribed into complementary DNA (cDNA) in accordance to the instructions of the cDNA synthesis kit (K1622; Fermentas Inc., Ontario, CA, USA). The expression of miR-21 was measured using the TaqMan miRNA kit (Ambion, Austin, TX, USA) with U6 as the internal control, and the expression of IL-12A and XIST was determined using the Prime Script RT-PCR kit (Takara, Shiga, Japan) with glyceraldehyde-3-phosphate dehydrogenase (GAPDH) as the internal control. The primer sequences are listed in Table 1. The $2^{-\Delta\Delta Ct}$ method was used to calculate the relative mRNA expression: $\Delta\Delta CT = \Delta Ct_{\text{experimental group}} - \Delta Ct_{\text{control group}}$, $\Delta Ct = Ct_{\text{target gene}} - Ct_{\text{internal control}}$. The experiment was repeated three times.

2.12. Western blot analysis

The total protein was extracted from BALF or PMNs using radio immunoprecipitation assay (RIPA) lysis buffer (R0010, Beijing Solarbio Science & Technology Co., Ltd. (Beijing, China) containing phenylmethylsulfonyl (PMSF). A total of 50 μg proteins were dissolved in 2 × sodium dodecyl sulfate (SDS) loading buffer and boiled at 100 °C for 5 min, followed by SDS-polyacrylamide gel electrophoresis (PAGE). Next, the proteins were transferred onto the polyvinylidene fluoride (PVDF) membrane by wet transfer method. The membrane was then blocked using 5% skimmed milk at room temperature for 1 h, and incubated at 4 °C overnight with the addition of the primary antibodies to GAPDH (ab8245, 1: 10,000), IL-12A (ab131039, 1: 1000), Cit-H3 (ab219407, 1: 1000). All antibodies were from Abcam Inc. (Cambridge, UK). After being rinsed with Tris-buffered saline

Table 1
Primer sequences for reverse transcription quantitative polymerase chain reaction.

Gene	Primer sequence (5′ - 3′)
miR-21	F: AAATTGGGAGGACTCCAAGC
	R: GAAGGAAAAAGTATGTCAGTGCAA
U6	F: AATTGGAACGATACAGAGAAGATTAGC
	R: TATGGAACGCTTCACGAATTTG
IL-12A	F: TGGCTACTAGAGAGACTTCTTCCACAA
	R: GCACAGGGTCATCAAAGAC
GAPDH	F: ACACATGGCCATCACTGCC
	R: GCCTGCTTCACCACCTTCTTG
XIST	F: CTCTCCATTGGGTTCAC
	R: GCGGCAGGTCTTAAGAGATGAG

Notes: F, forward; R, reverse; miR-21, microRNA-21; IL-12A, interleukin-12A; GAPDH, glyceraldehyde-3-phosphate dehydrogenase; XIST, X-inactive specific transcript.

Tween-20 (TBST) three times, the membrane was incubated with HRP-conjugated secondary antibody for 1 h, followed by exposure and imaging using the enhanced chemiluminescence (ECL) detection kit (BB-3501, Amersham Pharmacia, Piscataway, NJ, USA). Images were captured through the Bio-Rad image analysis system (Bio-Rad Inc., Hercules, CA, USA). The relative protein expression was analysed by the Quantity One v4.6.2 software. The experiment was repeated three times.

2.13. Dual luciferase reporter assay

The synthetic 3′UTR fragment of genes was inserted into the pMIR-reporter (Huayueyang Biotechnology Co., Ltd., Beijing China) using two endonuclease sites Spe I and Hind III. The mutant (Mut) site of complementary sequence of the seed sequence was designed based on the IL-12A-wild type (Wt). After restrictive endonuclease digestion, the target fragment was inserted into the pMIR-reported using T4 DNA ligase. The recombinant luciferase reporter plasmids IL-12A-Wt and IL-12A-Mut with the correct sequences were respectively co-transfected with miR-21 into human embryonic kidney 293T cells (CRL-1415, Shanghai Xin Yu Biological Technology Co., Ltd., Shanghai, China). After 48 h of transfection, the PMNs were lysed, and the luciferase activity was measured using a Glomax20/20 luminometer (Promega Corp., Madison, WI, USA) based on the instructions of the luciferase detection kit (RG005, Beyotime Biotechnology Co., Shanghai, China). The interaction between XIST and miR-21 was evaluated using the same method. The experiment in each group was repeated three times.

2.14. RNA-pull down

Biotinylated Bio-miR-21-Wt and Bio-miR-21-Mut as well as the corresponding Bio-NC (50 nM each) were transfected into PMNs, respectively. After 48 h, the PMNs were collected, washed with PBS, incubated with the specific lysis buffer (Ambion, Austin, TX, USA) for 10 min, and centrifuged at 14,000 × g to collect the supernatant. The protein lysate was incubated along with the M-280 streptavidin-coated magnetic beads (S3762, Sigma-Aldrich Chemical Company, St Louis MO, USA), which was pre-coated with RNase-free BSA and yeast tRNA (TRNABAK-RO, Sigma-Aldrich Chemical Company, St Louis MO, USA). The beads were incubated at 4 °C for 3 h and washed two times with precooled lysis buffer, three times with low-salt buffer, and one time with high-salt buffer. The immunoprecipitated RNA was purified using the Trizol method, and the expression of XIST was quantified by RT-qPCR.

2.15. RNA binding protein immunoprecipitation (RIP)

The PMNs were lysed using the lysis buffer containing 25 mM Tris−HCl (pH = 7.4), 150 mM NaCl, 0.5% NP-40, 2 mM ethylenediaminetetraacetic acid, 1 mM NaF and 0.5 mM dithiothreitol supplemented with the mixture of RNasin (Takara Biotechnology Ltd., Dalian, Liaoning, China) and protease inhibitor (B14001a, Roche Diagnostics, Indianapolis, IN, USA). The cell lysate was centrifuged at $12,000 \times g$ for 30 min, and the supernatant was incubated with the antibody to argonaute 2 (Ago2) magnetic beads (130−061−101, Shanghai univ-bio Inc., Shanghai, China) or the antibody to IgG magnetic beads at 4 °C for 4 h. The beads were washed three times with the washing buffer containing 50 mM Tris−HCl, 300 mM NaCl (pH = 7.4), 1 mM MgCl 2 and 0.1% NP-40). RNA was extracted from the magnetic beads using the Trizol method, and the expression of XIST and miR-21 was quantified by RT-qPCR.

2.16. Statistical analysis

Statistical analysis was conducted using the SPSS 19.0 software (IBM Corp. Armonk, NY, USA). All data were subjected to normal distribution test and variance homogeneity test. The measurement data conforming to normal distribution were presented as mean ± standard deviation and those not conforming to normal distribution or variance homogeneity were expressed as interquartile range. The data between two groups were compared using an unpaired t-test. One-way analysis of variance (ANOVA), followed by Tukey's post hoc test was used to analyze the variance of multiple groups with normal distribution and equal variances. Brown-Forsythe and Welch analysis of variance, followed by Tamhane's post hoc test was used to analyze the variance of multiple groups with unequal variances. The data with skewed distributions were tested using non-parametric test (Kruskal-Wallis test). $p < 0.05$ was used as the cut-off for statistically significant differences.

3. Results

3.1. miR-21 is downregulated in PGD and NET formation induces PGD after lung transplantation

To assess the consequence of lung transplantation on miR-21 expression levels in the context of PGD, we performed RT-qPCR. Intriguingly, in comparison to the non-PGD cohort, miR-21 expression was significantly decreased in the PGD patient cohort after lung transplantation, and expression levels were negatively associated with the PGD grade (Fig. 1a, b). In contrast, the levels of pro-inflammatory factors (IL-6, CXCL10, CCL2) and chemokine (IL-8) were higher in the PGD patients than those in non-PGD ones (Fig. 1c). Next, the cell population and number of PMNs in BALF of PGD and non-PGD patients were determined, whereas macrophages were found to be the major leukocyte population in BALF of non-PGD patients, PMNs were the main leukocyte population in BALF of PGD patients (Fig. 1d). Additionally, to comparatively assess the NET release and NET formation, we performed immunofluorescence staining. Our results revealed that the level of free DNA was elevated in the PGD patients as compared to that in the non-PGD patients (Fig. 1e). Furthermore, compared with the BAL cells of non-PGD patients, the expression of miR-21 was also reduced in BAL cells of PGD patients (Fig. 1f), as revealed by RT-qPCR. Taken together, these findings provide evidence that miR-21 is poorly expressed in PGD patients and posit NETs as a plausible pathogenic factor for PGD occurrence.
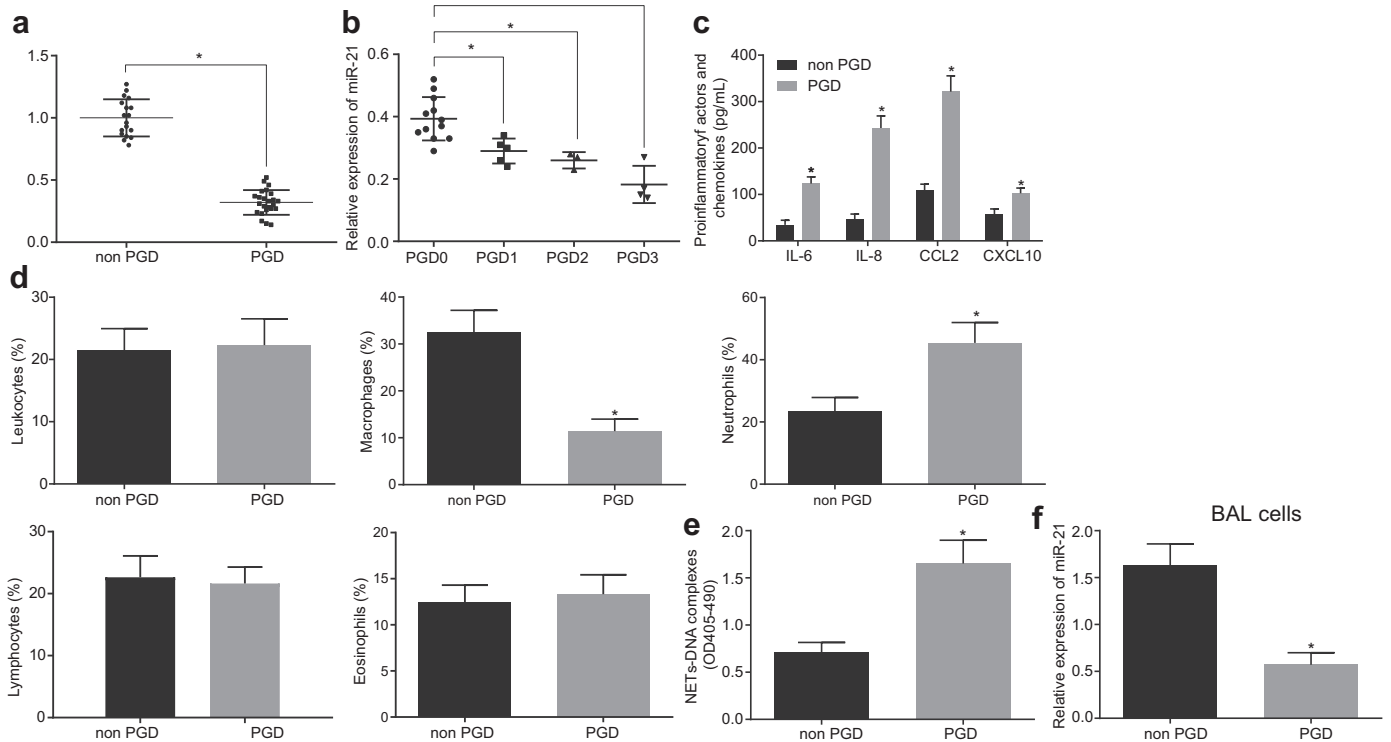

Fig. 1. miR-21 is poorly expressed in BALF of PGD patient where NET is a contributor for PGD. a, miR-21 was poorly expressed in BALF of PGD patients determined by RT-qPCR; b, miR-21 expression was conversely correlated to PGD grades, as detected by RT-qPCR; c, the expression of IL-6, CXCL10, CCL2, and IL-8 was higher in BALF of PGD than that in non-PGD patients, as measured by ELISA; d, the cell population of leukocytes was increased whilst that of macrophages was diminished in BALF of PGD patients; e, the level of free DNA was promoted in BALF of PGD patients, as detected by immunofluorescence staining; f, miR-21 expressed at a low level in BAL cells. All data were presented as mean ± standard deviation. The data between two groups were compared and analysed using unpaired t-test; $n = 18$ (non-PGD patients); $n = 24$ (PGD patients); * $p < 0.05$, compared with the non-PGD patients or PGD0 grade patients.

3.2. miR-21 ameliorates PGD after lung transplantation

To assess the consequence of modulating miR-21 levels, we transduced LV-miR-21 into the rats treated with PCI to restore the expression of miR-21. Firstly, we detected the expression of miR-21 in the sham-operated and PCI rats by RT-qPCR, and showed that the expression of miR-21 in the PCI rats was indeed significantly lower than that in the sham-operated rats, and that transduction with LV-miR-21 was able to restore expression of miR-21 in PCI rats (Fig. 2a). Blood gas analysis to measure the level of pO_2 demonstrated that rats treated with PCI had a reduced pO_2 level with oxygenation injury versus the sham-operated rats. LV-miR-21 transduction, however, resulted in enhanced pO_2 level in the rats treated with PCI (Fig. 2b). In addition, the treatment of PCI led to a higher W/D ratio of lung tissues, whilst the transduction of LV-miR-21 reduced the W/D ratio in the rats treated with PCI (Fig. 2c). Next, we scored lung injury using the semi-quantitative method, and demonstrated that compared to the rats treated with PCI and LV-NC, those treated with PCI and LV-miR-21 presented an attenuated lung injury score (Fig. 2d). The pathological changes of the lung tissues were then detected by HE staining, and revealed evidence of lung injury, such as interstitial space, pulmonary hemorrhage, alveolar edema, leukocyte infiltration upon PCI treatment (Fig. 2e). MGG coloration for determining cell population indicated an increased number of PMNs and a decreased number of macrophages in response to PCI treatment. When transduced with LV-miR-21 in a PCI setting, however, a reduced number of PMNs and an elevated number of macrophages were detected relative to the LV-NC controls (Fig. 2f). ELISA revealed enhanced levels of pro-inflammatory factors (IL-6, CXCL10, CCL2) and the chemokine IL-8 in PCI-treated rats, and this effect was suppressed upon LV-miR-21

transduction (Fig. 2g). Taken together, these results indicate that miR-21 alleviates PGD post lung transplantation.

3.3. miR-21 alleviates PGD by repressing NET formation

To explore the mechanism by which miR-21 influences PGD, we performed co-localization experiments by immunofluorescence staining of cit-H3 and NE in the BALF of rats after lung transplantation. We found that the NET level was increased after PCI treatment, but decreased in response to the transduction of LV-miR-21 after the treatment of PCI (Fig. 3a). Furthermore, as indicated by ELISA, PCI treatment led to elevated levels of NET-DNA complexes, which again, was decreased in response to transduction of LV-miR-21 (Fig. 3b). We also measured the protein expression of cit-H3 in BALF using western blot analysis and showed that cit-H3 is upregulated in response to the treatment of PCI, but this upregulation was attenuated by the transduction of LV-miR-21 (Fig. 3c).

In order to verify the role of miR-21 in PGD in vitro, we conducted a gain-of-function experiment where we transfected PMNs with a miR-21 mimic. This in vitro assay further demonstrated that PMNs transfected with miR-21 mimic exhibited a markedly decreased level of NET-DNA complexes over the non-targeting control (Fig. 3d). In addition, we also noticed a reduced number of filamentous and green-stained intercellular DNA in miR-21 mimic-treated PMNs than those in mimic NC-treated PMNs (Fig. 3e). Further, we observed a decreased apoptotic rate in PMNs after PMA treatment (Fig. 3f), but this effect was reversed upon overexpression of miR-21 in PMA-treated PMNs (Fig. 3g). All in all, these results suggest that the inhibitory effect of miR-21 on PGD may be correlated to the suppression of NET formation.
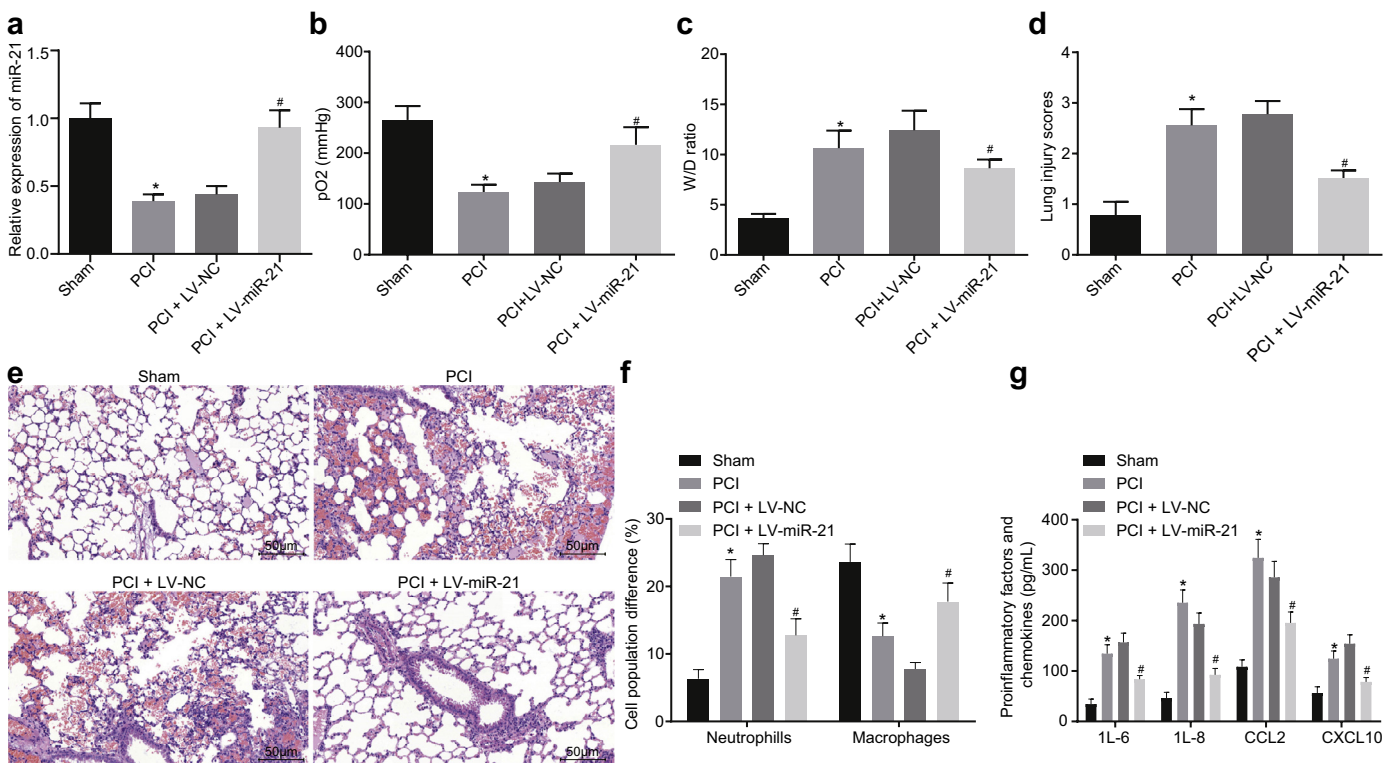

Fig. 2. miR-21 alleviates PGD after lung transplantation. a, LV-miR-21 promotes the expression of miR-21 in PCI rats; b, the pO_2 level was increased by LV-miR-21, as measured by the blood gas analyser; c, the W/D ratio of the left lung tissues was reduced by LV-miR-21 in PCI rats; d, the lung injury score was lowered by LV-miR-21, as assessed by the semi-quantitative method; e, the pathological changes of the left lung tissues were alleviated by LV-miR-21 observed by HE staining (200 ×); f, the cell population of leukocytes was reduced whilst that of macrophages was restored after treatment with LV-miR-21 in PCI rats; g, the levels of IL-6, CXCL10, CCL2 and IL-8 was hampered in BALF of PCI rats after treatment with LV-miR-21. All data were presented as mean ± standard deviation. The data with skew distribution were tested using non-parametric test (Kruskal-Wallis test). One-way analysis of variance was used to analyze the variance of multiple groups with normal distribution. Brown-Forsythe and Welch analysis of variance, followed by Tamhane's post hoc test, was used to analyze the variance of multiple groups with unequal variances. $n = 9$; *$p < 0.05$, compared with the sham group; #$p < 0.05$, compared with the PCI + LV-NC group.
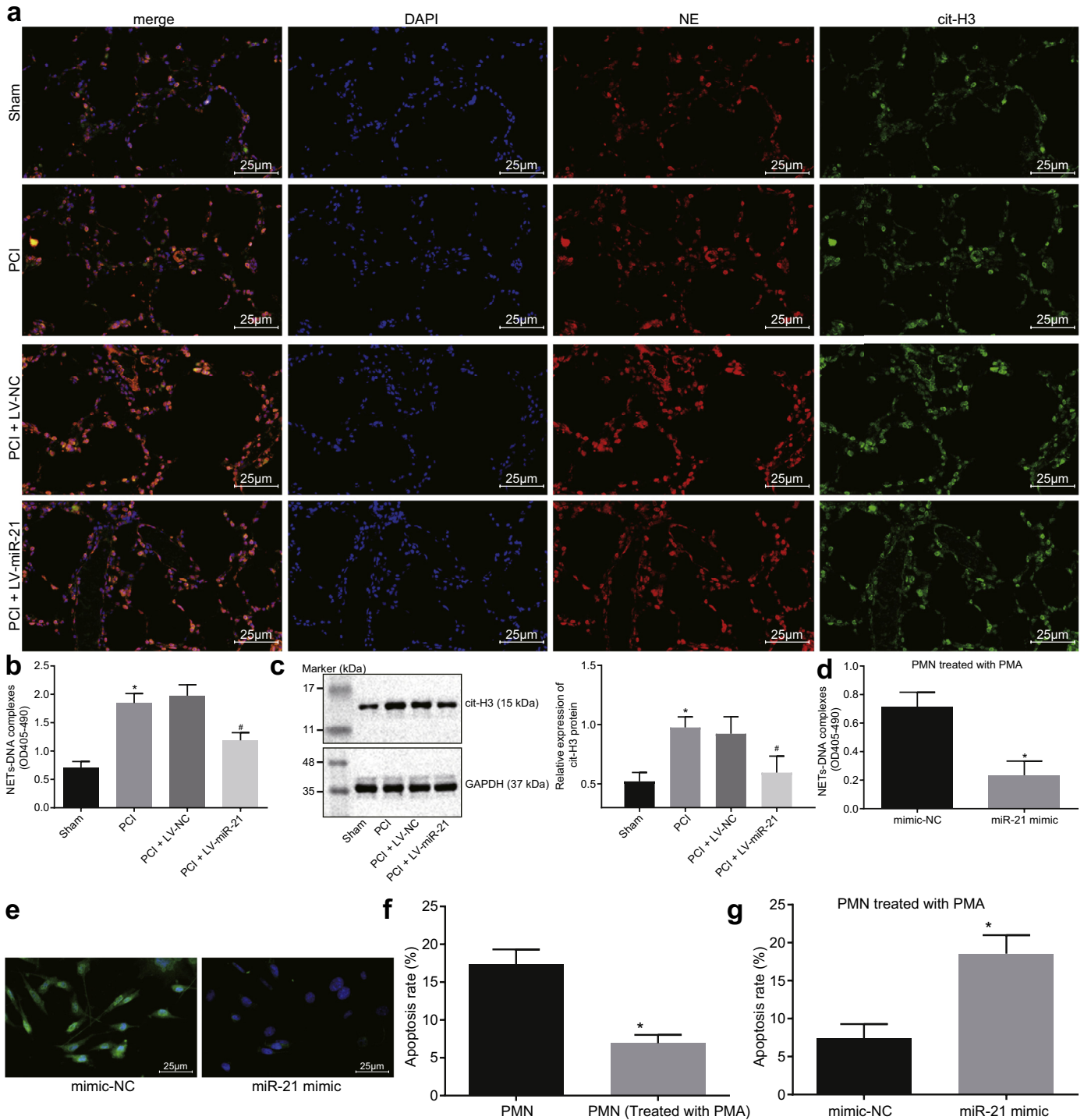
Fig. 3. miR-21 alleviates PGD after lung transplantation by repressing NET formation. a, the level of NET was downregulated by LV-miR-21, as detected by immunofluorescence staining (400 ×); b, the level of NET-DNA in BALF of rats was decreased after treatment with LV-miR-21, as determined by ELISA; c, the protein expression of cit-H3 was decreased in BALF after treatment with LV-miR-21, as detected by western blot analysis; (*$p < 0.05$, compared with the sham group; #$p < 0.05$, compared with the PCI + LV-NC group); d, the content of NET-DNA in PMNs transfected with miR-21 mimic was inhibited, as measured using ELISA; e, the level of free DNA in PMNs was suppressed after transfection with miR-21 mimic, as detected by immunofluorescence staining (400 ×); f, the apoptosis rate of PMNs was lowered by PMA treatment, as detected by flow cytometry (*$p < 0.05$, compared with the PMA-treated PMNs); g, the apoptosis rate of PMA-treated PMNs after transfection with miR-21 mimic was increased, as determined by flow cytometry. All data were presented as mean ± standard deviation. The data between two groups were compared and analysed using unpaired *t*-test; one-way analysis of variance followed by Tukey's post hoc test was used to analyze the variance of multiple groups with normal distribution. Brown-Forsythe and Welch analysis of variance, followed by Tamhane's post hoc test, was used to analyze the variance of multiple groups with unequal variances; the experiment in panel D - G was repeated three times; *$p < 0.05$, compared with the sham, PMNs, or mimic-NC groups; #$p < 0.05$, compared with the PCI + LV-NC group.

3.4. miR-21 specifically binds to IL-12A to inhibit NET formation

We determined a binding relationship between miR-21 and IL-12A using a biological prediction tool Targetscan (Fig. 4a), and were able to validate our *in silico* finding using a dual luciferase reporter assay. Briefly, whilst the luciferase activity of IL-12A-Mut was not affected significantly with the co-transfection of miR-21 mimic ($p > 0.05$), the luciferase activity of IL-12A-Wt was significantly attenuated when co-transfected with miR-21 mimic ($p < 0.05$; Fig. 4b).
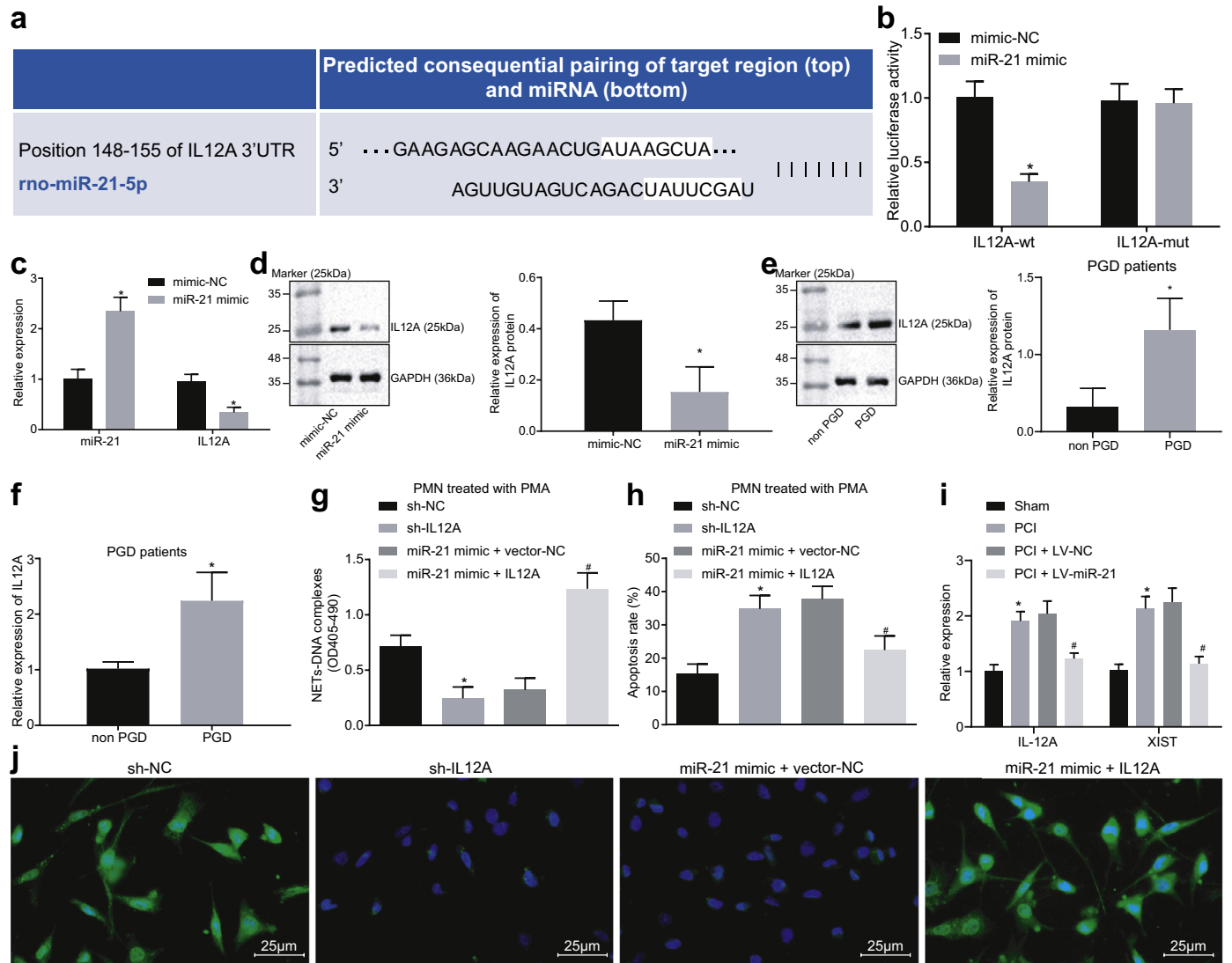
Fig. 4. IL-12A is a target gene of miR-21, and can reverse the inhibitory effect of miR-21 on NET formation. a, there were binding sites between miR-21 and IL-12A, as predicted on the Tar-getScan software (http://www.targetscan.org/); b, IL12A-wt expression was repressed by miR-21 mimic verified by the dual luciferase reporter assay; c, the mRNA expression of IL-12A in PMNs following transfection with miR-21 mimic was inhibited, as detected by RT-qPCR; d, the protein expression of IL-12A was suppressed in response to the treatment with miR-21 mimic, as determined by western blot analysis; e, the protein expression of IL-12A in BALF of PGD patients was enhanced, as determined by western blot analysis; f, the mRNA expression of IL-12A in BALF of PGD patients was facilitated, as determined by RT-qPCR; g, the content of NET-DNA in PMA-treated PMNs transfected with sh-IL-12A or miR-21 mimic was reduced, as assessed by ELISA; h, the apoptosis rate was promoted in PMA-treated PMNs transfected with sh-IL-12A or miR-21 mimic, as detected by flow cytometry; i, the mRNA expression of IL-12A in BALF of rats was diminished after miR-21 mimic treatment, as determined by RT-qPCR; j, the content of free DNA was decreased in PMNs transfected with sh-IL-12A or miR-21 mimic, as detected by immunofluorescence staining (400 ×). All data were presented as mean ± standard deviation. The data between two groups were compared and analysed using unpaired t-test; one-way analysis of variance followed by Tukey's post hoc test was used to analyze the variance of multiple groups with normal distribution. Brown-Forsythe and Welch analysis of variance, followed by Tamhane's post hoc test, was used to analyze the variance of multiple groups with unequal variances; the experiment was repeated three times; in panel f, n = 18 (non-PGD patients); n = 24 (PGD patients); $^*p < 0.05$ compared with the miR-21 mimic NC, non-PGD, or sh-NC groups; $^#p < 0.05$, compared with the miR-21 mimic + vector NC group.

The regulatory effects of miR-21 and IL-12A were then further examined using loss- and gain- of-function approaches. The miR-21 expression and the mRNA and protein expression of IL-12A were determined by RT-qPCR and western blot analysis. We found that the expression of IL-12A was downregulated in PMNs transfected with miR-21 mimic relative to that of the PMNs transfected with mimic-NC ($p < 0.05$) (Fig. 4c, d). We further determined that the mRNA and pro-tein expression of IL-12A was upregulated in BALF of the PGD patients *versus* that in the BALF of the non-PGD patients (Fig. 4e, f). Next, we demonstrated that the content of NET-DNA was lower in PMA-treated PMNs upon silencing of IL-12A with sh-IL-12A transfection, but higher in PMA-treated PMNs harboring overexpressed miR-21 and IL-12A over those harboring overexpressed miR-21 only (Fig. 4g). Further-more, the downregulation of IL-12A in PMA-treated PMNs led to an elevated apoptosis rate, whereas upregulation of IL-12A in the same

setting attenuated the miR-21 mimic-induced apoptosis (Fig. 4h). The expression of IL-12A in BALF of rats was then determined by RT-qPCR, and revealed a decreased expression of IL-12A upon miR-21 treatment (Fig. 4i). Finally, immunofluorescence staining showed a reduced num-ber of filamentous and green-stained intercellular DNA in response to sh-IL-12A treatment, and an elevated number upon dual overexpres-sion of miR-21 mimic and IL-12A relative to miR-21 mimic overex-pression alone (Fig. 4j). In conclusion, we show that miR-21 inhibits NET formation by targeting IL-12A.

3.5. LncRNA XIST elevates the expression of IL-12A by acting as a ceRNA of miR-21

It was predicted that there existed binding sites between miR-21 and XIST (Fig. 5a). We again utilized the dual luciferase reporter assay
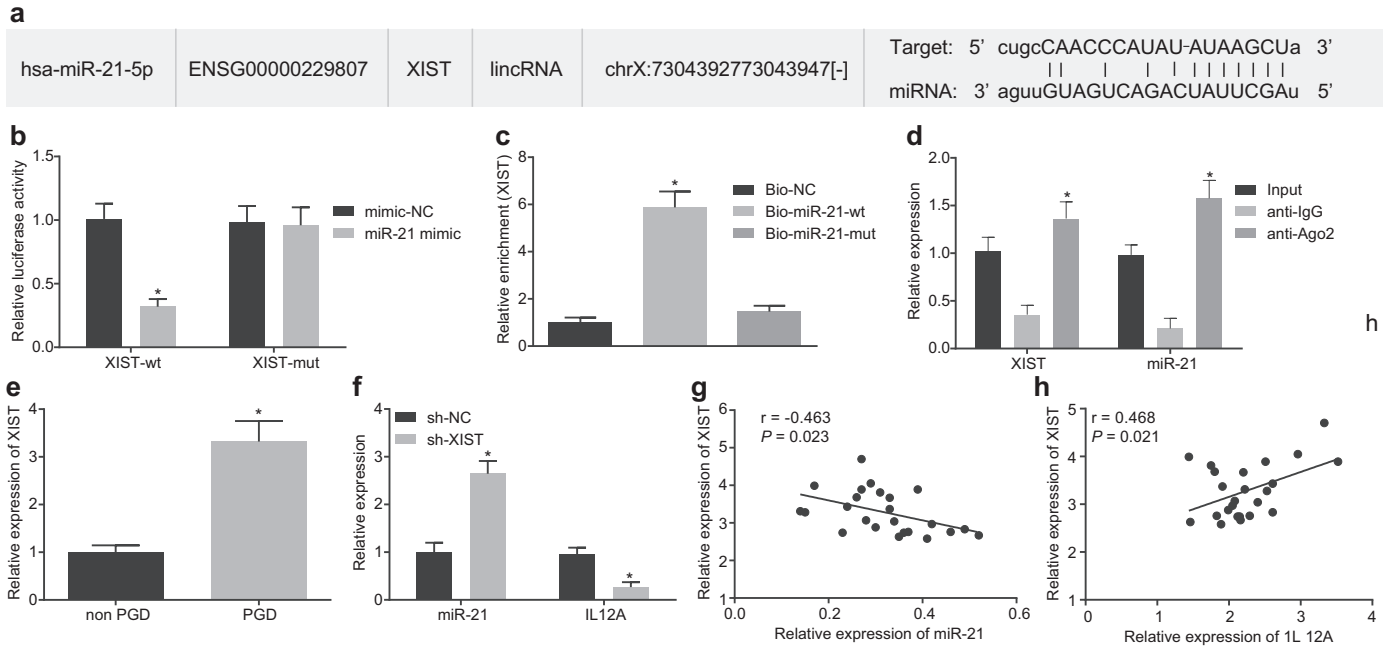
Fig. 5. LncRNA XIST upregulates IL-12A by binding to miR-21. a, there were binding sites between miR-21 and XIST, according to online prediction; b, the luciferase activity of XIST-wt was inhibited by miR-21 mimic, as confirmed by the dual luciferase reporter assay; c, XIST was pulled-down by miR-21-Mut in RNA pull-down assay; d, the expression of miR-21 and XIST coprecipitated with Ago2 magnetic beads was enhanced in the RIP assay; e, XIST was upregulated in BALF of PGD patients, as measured by RT-qPCR; f, the expression of miR-21 was promoted and IL-12A expression was suppressed in PMNs after the suppression of XIST, as measured by RT-qPCR; g, there was a negative correlation between miR-21 and XIST, as determined by the correlation analysis; h, IL-12A and XIST were positively correlated, as determined by the correlation analysis. All data were presented as mean ± standard deviation. The data between PGD patients ($n = 24$) and non-PGD patients ($n = 18$) in panel e were compared and analysed using unpaired t-test; one-way analysis of variance followed by Tukey's post hoc test was used to analyze the variance of multiple groups with normal distribution. Brown-Forsythe and Welch analysis of variance, followed by Tamhane's post hoc test, was used to analyze the variance of multiple groups with unequal variances; the experiment was repeated three times; $^*p < 0.05$, compared with the mimic-NC, anti-IgG, or sh-NC groups.

to show that in XIST-Wt cells, mimic-NC had no effect on luciferase activity of XIST, but after miR-21 mimic transfection, the luciferase activity of XIST was significantly inhibited. In XIST-Mut, both treatments had no effect on luciferase activity of XIST, indicating that there were specific binding sites between miR-21 and XIST (Fig. 5b). We then sought to explore the interaction between miR-21 and XIST by conducting RNA pull-down and RIP assays. Encouragingly, we found an enriched level of XIST pulled down by miR-21-Wt over miR-21-Mut, which also validated a binding interaction of miR-21 with XIST (Fig. 5c). Next, the RIP assay showed that the expression of XIST and miR-21 bound with Ago2 was elevated compared to those bound with IgG, again demonstrating that miR-21 interacts with XIST (Fig. 5d). Further we also detected a high expression of XIST in the BALF of PGD patients (Fig. 5e). We then demonstrated that the deletion of XIST by transfection of sh-XIST enhanced miR-21 expression but suppressed IL-12A expression (Fig. 5f). Finally, the correlation analysis indicated that XIST was negatively correlated with miR-21, but positively correlated with IL-12A (Fig. 5g, h). In summary, the above results provide evidence that XIST can competitively bind to miR-21 to upregulate the expression of IL-12A.

3.6. XIST silencing upregulates miR-21 but downregulates IL-12A, alleviating PGD after lung transplantation through the inhibition of NET formation

To further analyze the regulatory effects of XIST, miR-21 and IL-12A on PGD *in vivo*, we delivered sh-XIST, an IL-12A overexpression vector and a miR-21 sponge respectively, into rats following lung transplantation. RT-qPCR results revealed that XIST was poorly expressed before and during single lung transplantation, but overexpressed after single lung transplantation. Further examination of XIST expression in PCI rats illustrated that the sh-XIST transfection followed by treatments of sponge control, vector-NC and IL-12A all

significantly diminished XIST expression, but sh-XIST plus miR-21 sponge treatment restored XIST expression (Fig. 6a). To comparatively assess pulmonary edema of the rats, the W/D ratio was then measured and revealed a higher W/D ratio for the combination of sh-XIST and miR-21 sponge delivery over the combination of sh-XIST and sponge control delivery. In addition, the W/D ratio was higher in response to the treatment with sh-XIST and IL-12A overexpression vector over those treated with sh-XIST and vector NC (Fig. 6b). Next, HE staining exhibited that lung injury was aggravated after treatment with sh-XIST and miR-21 sponge relative to treatment with sh-XIST and sponge control (Fig. 6c). The lung injury was then scored using the semi-quantitative method, and was found to be higher following treatment with sh-XIST and IL-12A overexpression vector than after treatment with sh-XIST and vector NC (Fig. 6d).

Masson staining analysis illustrated that dual treatment with sh-XIST and vector-NC, sh-XIST and sponge resulted in thickened muscular layer of bronchial wall membrane, disorderly arrangement of smooth muscle, and obvious fibrous hyperplasia. The bronchial wall was thickened and exhibited fibrosis, and a large number of blue-stained thick fibers were found around the bronchi and blood vessels, in addition to more serious destruction of the original structure due to the thick collagen and fibrotic scar tissue in the presence of sh-XIST and miR-21 sponge, sh-XIST and IL-12A (Fig. 6e, f).

Furthermore, using ELISA, we determined higher levels of pro-inflammatory factors IL-6, CXCL10, CCL2 and the chemokine IL-8 in response to treatment with sh-XIST and miR-21 sponge *versus* the sh-XIST and sponge control. Interestingly, the increase in the levels of the aforementioned factors was also detected when treated with sh-XIST and IL-12A overexpression vector in comparison with the combined treatment with sh-XIST and vector-NC (Fig. 6g). MGG coloration revealed a higher number of PMNs in response to the transduction of sh-XIST and miR-21 sponge than that of sh-XIST and sponge control, and a similar observation was made for the treatment
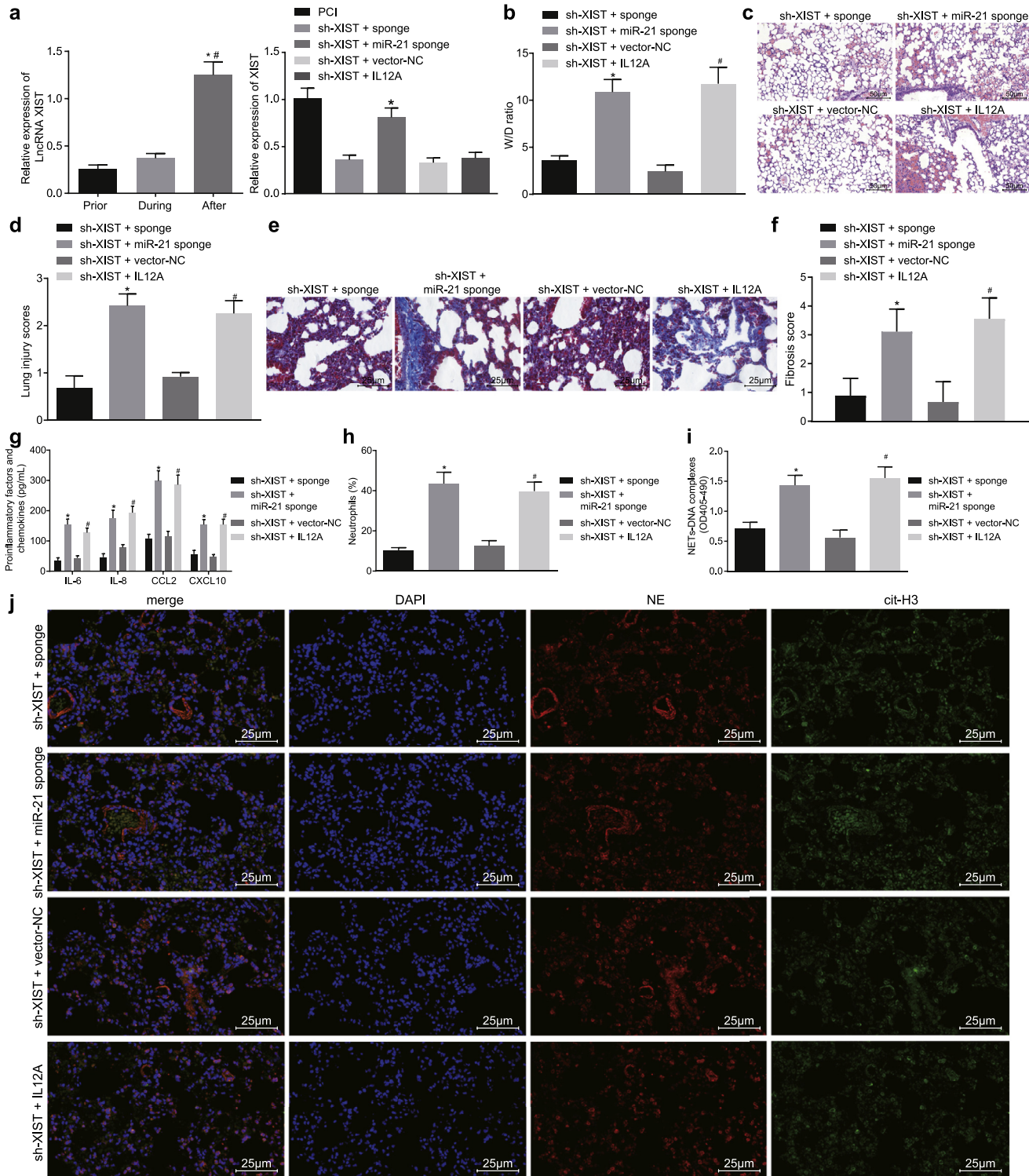
Fig. 6. Silencing of XIST inhibits the expression of IL-12A by upregulating miR-21 to suppress NET formation and ultimately to ameliorate PGD after lung transplantation. a, XIST was poorly expressed before and during the single lung transplantation, whilst it was overexpressed after single lung transplantation where *p < 0.05, compared with before the single lung transplantation; #p < 0.05, compared with during the single lung transplantation; b, the W/D ratio of the left lung tissues was increased in rats after transduction of sh-XIST and IL-12A overexpression vector; c, pathological changes of the left lung tissues were aggravated in rats after transduction of sh-XIST and IL-12A overexpression vector, as detected by HE staining (200 ×); d, lung injury scores of the rats was promoted after transduction of sh-XIST and IL-12A overexpression vector using the semi-quantitative method; e, Masson staining of lung tissue in response to transduction of sh-XIST and IL-12A overexpression vector; f, pulmonary fibrosis score in response to transduction of sh-XIST and IL-12A overexpression vector; g, the expression of IL-6, IL-8, CCL2, and CXCL10 in BALF of the rats was increased in response to transduction of sh-XIST and IL-12A overexpression vector, as measured by ELISA; h, the number of PMNs was promoted following transfection of sh-XIST and IL-12A overexpression vector, as assessed by MGG coloration; i, the content of NET-DNA in BALF of rats was increased after transduction of sh-XIST and IL-12A overexpression vector, as determined by ELISA; j, the level of NET was facilitated following transduction of sh-XIST and IL-12A overexpression vector, as examined by immunofluorescence staining (400 ×). All data were presented as mean ± standard deviation. The data in panel d were tested using non-parametric test (Kruskal-Wallis test); one-way analysis of variance followed by Tukey's post hoc test was used to analyze the variance of multiple groups with normal distribution. Brown-Forsythe and Welch analysis of variance, followed by Tamhane's post hoc test, was used to analyze the variance of multiple groups with unequal variances; n = 9; *p < 0.05, compared with the sh-XIST + sponge group; #p < 0.05, compared with the sh-XIST + vector NC group.
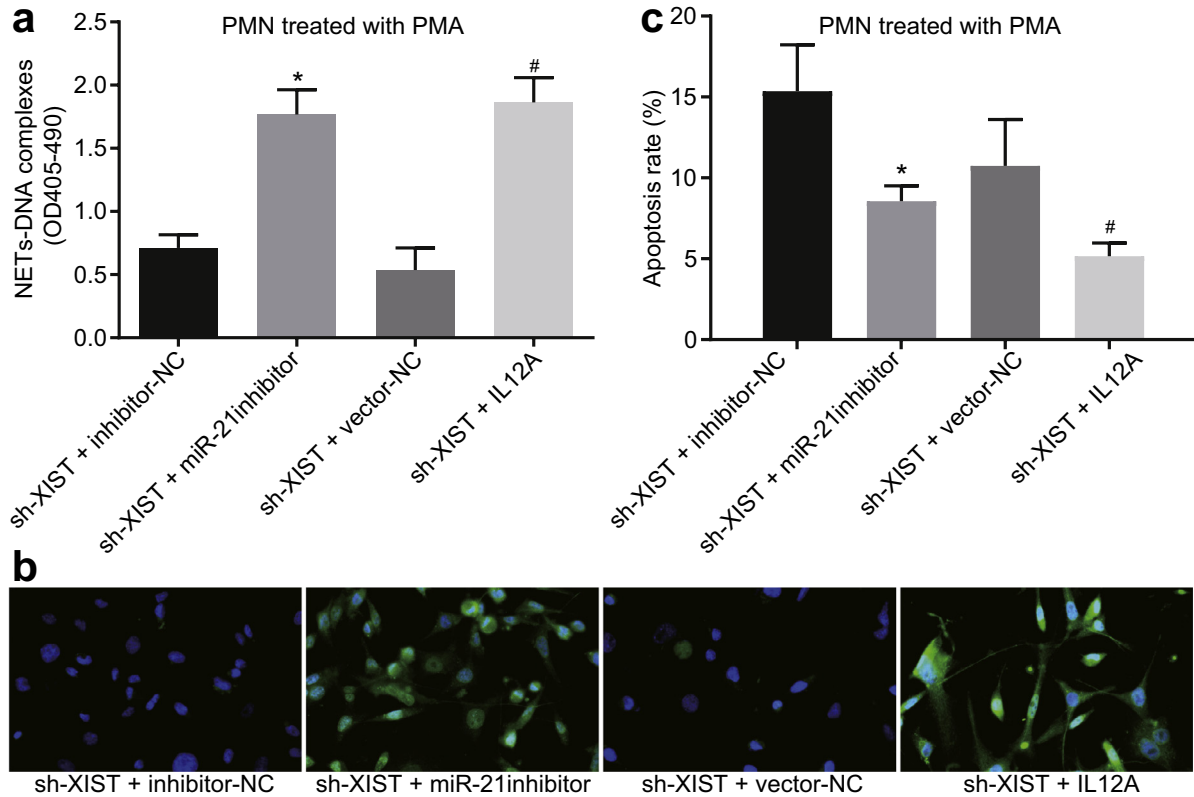
Fig. 7. LncRNA XIST silencing decreases IL-12A expression to suppress NET formation in PMNs *in vitro* by elevating miR-21. a, the content of NET-DNA was elevated in PMA-treated PMNs after transfection with sh-XIST and IL-12A overexpression vector, as determined by ELISA; b, the content of free DNA in PMNs was increased after transfection with sh-XIST and IL-12A overexpression vector, as detected by immunofluorescence staining; c, the apoptosis rate of PMA-treated PMNs was promoted after transfection with sh-XIST and IL-12A overexpression vector, as determined by flow cytometry. All data were presented as mean ± standard deviation. Comparison of data among multiple groups was conducted using one-way ANOVA; the experiment was repeated three times; $^*p < 0.05$, compared with the sh-XIST + inhibitor NC group; $^\#p < 0.05$, compared with the sh-XIST + vector NC group.

of sh-XIST and IL-12A overexpression vector compared to the treatment of sh-XIST and vector NC (Fig. 6h). Next, we found that treatment with sh-XIST and miR-21 sponge led to an increased content of NET-DNA in BALF in comparison to the treatment with sh-XIST and sponge control. XIST silencing plus IL-12A overexpression also contributed to a higher content of NET-DNA in BALF over XIST silencing alone, as assessed by ELISA (Fig. 6i). Finally, immunofluorescence staining suggested that the NET level was elevated by the transduction of sh-XIST and miR-21 sponge over the transduction of sh-XIST and sponge control. Similarly, the combination of XIST silencing and IL-12A overexpression led to an enhanced NET level than XIST silencing alone (Fig. 6j). The above results demonstrate that the downregulated expression of XIST or over-expression of miR-21 suppresses IL-12A and represses NET formation, which is beneficial for PGD alleviation.

3.7. LncRNA XIST silencing decreases IL-12A expression to suppress NET formation in vitro by elevating miR-21

To further evaluate the mechanistic underpinnings of the effects of XIST/miR-21/IL-12A axis on NET formation we used a series of *in vitro* assays. First, we introduced the sh-XIST, IL-12A overexpression vector and miR-21 inhibitor respectively into the PMA-treated PMNs and found that the content of NET-DNA was remarkably elevated by the combined treatment with sh-XIST and miR-21 inhibitor or sh-XIST plus IL-12A overexpression vector in comparison with the combined treatment with sh-XIST plus inhibitor-NC or sh-XIST plus vector-NC, respectively (Fig. 7a). The results of immunofluorescence staining showed that XIST silencing along with miR-21 inhibition or XIST silencing plus IL-12A overexpression led to an increased number

of filamentous and green-stained intercellular DNA than XIST silencing alone (Fig. 7b). Next, using flow cytometry, we measured the apoptosis rate in PMA-treated PMNs and showed that PMA-treated PMNs transfected with sh-XIST and miR-21 inhibitor or those transfected with sh-XIST and IL-12A overexpression vector exhibited lower apoptosis rates in comparison to those transfected with sh-XIST and inhibitor-NC or sh-XIST and vector-NC, independently (Fig. 7c). Taken together, these results support the conclusion that inhibition of miR-21 or elevation of IL-12A reverses the effects of XIST silencing on NET formation.

4. Discussion

Despite some available immunosuppressive treatments, patients with PGD still suffer from worsened conditions [35]. With the ultimate goal of uncovering additional therapeutic targets for PGD, this study investigated the underlying mechanism by which XIST affects PGD. The findings in the current study provide evidence that XIST silencing downregulates IL-12A expression through the upregulation of miR-21, thereby inhibiting NET formation and ultimately alleviating PGD after lung transplantation.

Initially, we found that XIST and IL-12A were highly expressed, whilst miR-21 was poorly expressed in BALF and BAL cells of PGD patients. Aside from our evidence, IL-12A has been reported to be elevated in mice with pneumonia [36]. A previous study also demonstrated that patients with severe PGD after lung transplantation exhibit markedly downregulated expression of miR-21 [21], which is in line with our results. Notably, miR-21 upregulation has also been known to induce the transition of monocytes to fibrocytes through upregulated CCL2 in a murine cardiac allograft transplantation model
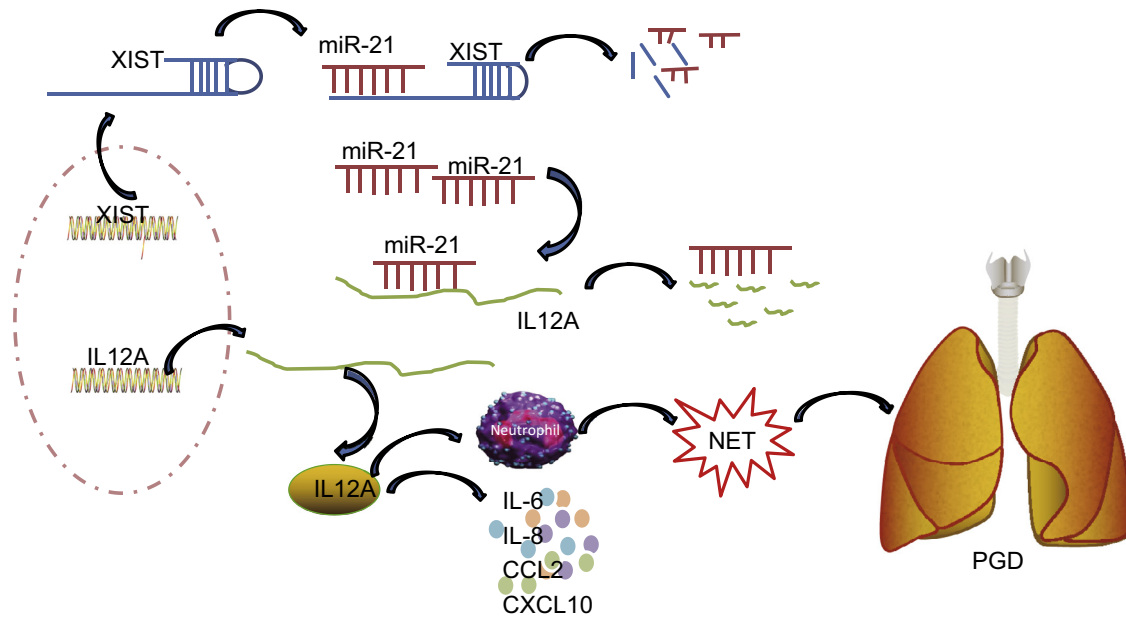
Fig. 8. Schematic representation of the regulatory network of XIST/miR-21/IL-12A during the NET formation in PGD following lung transplantation. XIST, as a ceRNA of miR-21, upregulates the expression of IL-12A, which induces NET formation and ultimately accelerates PGD after lung transplantation.

[37]. Additionally, enhanced circulating miR-21 expression is closely correlated to the progression of kidney and lung fibrosis [38,39]. Based on these premises, there is a possibility that XIST may regulate miR-21 and IL-12A in the development of PGD. Subsequently, it was found that XIST could serve as a ceRNA of miR-21, and IL-12A was a target gene of miR-21. It is widely known that many lncRNAs could serve as ceRNAs or regulatory sponges of miRNAs to mediate their expression and functions in human diseases [40]. For example, lncRNA XIST, as a ceRNA of miR-194−5p, is negatively correlated to the expression of miR-194−5p in hepatocellular carcinoma [41]. XIST has been demonstrated to be upregulated in lung cancer cells and its silencing leads to suppressed cancer progression by upregulating miR-140 and downregulating its target inhibitor of apoptosis-stimulating protein of p53 [42]. Additionally, there is a negative correlation between miR-21 and IL-12A, both of which are closely associated with inflammation [43]. Our experimental results showed that IL-12A was decreased and NET formation was increased after overexpression of miR-21, which indicated that IL-12A could promote NET formation. Some evidence has shown that the occurrence of PGD induces recruited and activated immune cells [1], which may be the reason for the increase of IL-12A in BALF and the increased IL-12A can promote NET formation in PMNs, thus exacerbating PGD.

PMNs, as the first line of defense against innate immunity, can produce inflammatory mediators, such as antimicrobial peptides, active oxygen, cytokines, etc. [44]. In addition, PMNs can release NET, a special mechanism that enables DNA to enter the extracellular environment [45]. Although PMNs play an essential role in defending against pathogenic microorganisms, excessive or long-term activation of PMNs can induce ALI [46]. Intriguingly, the findings of the current study demonstrated that miR-21 contributes to inhibited NET formation, downregulates the expression of pro-inflammatory factors (IL-6, CXCL10, and CCL2) and the chemokine IL-8, and promotes the apoptosis of PMNs. Excessive presence of NET formation can lead to aggravated immune responses as well as tissue injury [47]. miR-NAs are found to possess the ability to distinguish NET subunits and identify NET from adenocarcinoma and miR-21 elevation has been previously revealed in NET with low grade in metastatic tumours [48]. Inhibition of NET has also been reported to ameliorate PGD, and is thus being considered as a potential strategy for PGD treatment

[28]. Both CXCL10 and CCL2 have been indicated to be upregulated in PGD after lung transplantation [49]. In addition, miR-21 has been suggested to be an important negative regulator of inflammation in myocardial infarction [50]. Independently, it has been shown that neutrophils are elevated in response to the downregulation of miR-21 in allergic lungs [51]. In our study, further *in vivo* and *in vitro* investigations demonstrated that XIST silencing can inhibit NET formation through upregulation of miR-21. However, we also showed that inhibition of miR-21 and elevation of IL-12A reversed the effects of XIST silencing on NET formation. In a similar vein, a previous report posited that XIST suppression attenuates inflammatory pain through inhibiting the expression of Nav1.7 by serving as a ceRNA of miR-146a [52]. In addition, XIST has been highlighted to alleviate neuropathic pain by negatively mediating miR-137 but positively regulating tumor necrosis factor alpha-induced protein 1 (TNFAIP1), both of which are closely associated with inflammation [53]. These reports can provide supports for our finding.

5. Conclusion

The findings of the present study highlight that silencing of XIST inhibits NET formation, thus ultimately alleviating PGD after lung transplantation. Based on our results, we propose a network of XIST/ miR-21/IL-12A as an underlying regulatory mechanism mediating NET formation (Fig. 8). In conclusion, we see our study as laying the groundwork for further investigations having defined an interaction between XIST and miR-21 in PGD, which may lead to newer insights and novel therapeutic approaches in combating PGD. Looking ahead, more complicated regulatory pathways are awaiting further mechanistic validation and the support of clinical data, as well as detailed studies of the effects of miR-21 inhibition on ALI or relevant injuries in animal models.

Declaration of competing interest

The authors declare that they have no conflicts of interest.

Acknowledgments

Authors' contributions

Jiwei Li, Li Wei and Zhijun Han wrote the paper and conceived and designed the experiments; Zhong Chen and Quan Zhang analysed the data; Jiwei Li and Li Wei collected and provided the sample for this study. All authors have read and approved the final submitted manuscript.

References

[1] Suzuki Y, Cantu E, Christie JD. Primary graft dysfunction. Semin Respir Crit Care Med 2013;34(3):305–19.
[2] Porteous MK, Lee JC. Primary graft dysfunction after lung transplantation. Clin Chest Med 2017;38(4):641–54.
[3] Diamond JM, Kawut SM, Lederer DJ, et al. Elevated plasma clara cell secretory protein concentration is associated with high-grade primary graft dysfunction. Am J Transplant 2011;11(3):561–7.
[4] Lee JC, Christie JD, Keshavjee S. Primary graft dysfunction: definition, risk factors, short- and long-term outcomes. Semin Respir Crit Care Med 2010;31(2):161–71.
[5] Pelaez A, Mitchell PO, Shah NS, et al. The role of donor chronic alcohol abuse in the development of primary graft dysfunction in lung transplant recipients. Am J Med Sci 2015;349(2):117–23.
[6] Kolaczkowska E, Kubes P. Neutrophil recruitment and function in health and inflammation. Nat Rev Immunol 2013;13(3):159–75.
[7] Martinez NE, Zimmermann TJ, Goosmann C, et al. Tetrahydroisoquinolines: new inhibitors of neutrophil extracellular trap (NET) formation. Chembiochem 2017;18(10):888–93.
[8] Li H, Zhou X, Tan H, et al. Neutrophil extracellular traps contribute to the pathogenesis of acid-aspiration-induced ALI/ARDS. Oncotarget 2018;9(2):1772–84.
[9] Remijsen Q, Vanden Berghe T, Wirawan E, et al. Neutrophil extracellular trap cell death requires both autophagy and superoxide generation. Cell Res 2011;21(2):290–304.
[10] Emtiazjoo A, Shilling RA. Preventing the NET negative in primary graft dysfunction. Am J Respir Crit Care Med 2015;191(4):368–9.
[11] Samano MN, Fernandes LM, Baranauskas JC, et al. Risk factors and survival impact of primary graft dysfunction after lung transplantation in a single institution. Transplant Proc 2012;44(8):2462–8.
[12] Pelaez A, Force SD, Gal AA, et al. Receptor for advanced glycation end products in donor lungs is associated with primary graft dysfunction after lung transplantation. Am J Transplant 2010;10(4):900–7.
[13] Fang XY, Pan HF, Leng RX, Ye DQ. Long noncoding RNAs: novel insights into gastric cancer. Cancer Lett 2015;356(2 Pt B):357–66.
[14] Quinn JJ, Chang HY. Unique features of long non-coding RNA biogenesis and function. Nat Rev Genet 2016;17(1):47–62.
[15] Yang L, Long Y, Li C, et al. Genome-wide analysis of long noncoding RNA profile in human gastric epithelial cell response to helicobacter pylori. Jpn J Infect Dis 2015;68(1):63–6.
[16] Wei W, Liu Y, Lu Y, et al. LncRNA XIST promotes pancreatic cancer proliferation through miR-133a/EGFR. J Cell Biochem 2017;118(10):3349–58.
[17] Sun J, Pan LM, Chen LB, Wang Y. LncRNA XIST promotes human lung adenocarcinoma cells to cisplatin resistance via let-7i/BAG-1 axis. Cell Cycle 2017;16(21):2100–7.
[18] Jiang H, Zhang H, Hu X, Li W. Knockdown of long non-coding RNA XIST inhibits cell viability and invasion by regulating miR-137/PXN axis in non-small cell lung cancer. Int J Biol Macromol 2018;111:623–31.
[19] Cheng CJ, Bahal R, Babar IA, et al. MicroRNA silencing for cancer therapy targeted to the tumour microenvironment. Nature 2015;518(7537):107–10.
[20] Zhang W, Zhou T, Ma SF, et al. MicroRNAs implicated in dysregulation of gene expression following human lung transplantation. Transl Respir Med 2013;1(1).
[21] Xu Z, Sharma M, Gelman A, et al. Significant role for microRNA-21 affecting toll-like receptor pathway in primary graft dysfunction after human lung transplantation. J Heart Lung Transplant 2017;36(3):331–9.
[22] Qin S, Chen M, Ji H, et al. miR215p regulates type ii alveolar epithelial cell apoptosis in hyperoxic acute lung injury. Mol Med Rep 2018;17(4):5796–804.
[23] Wu Z, Lu H, Sheng J, Li L. Inductive microRNA-21 impairs anti-mycobacterial responses by targeting IL-12 and BCL-2. FEBS Lett 2012;586(16):2459–67.
[24] Sima X, Xu J, Li Q, et al. Gene-gene interactions between interleukin-12A and interleukin-12B with the risk of brain tumor. DNA Cell Biol 2012;31(2):219–23.
[25] Wang EY, Liang WB, Zhang L. Association between single-nucleotide polymorphisms in interleukin-12A and risk of chronic obstructive pulmonary disease. DNA Cell Biol 2012;31(9):1475–9.
[26] Sun J, Xue Q, Guo L, et al. Xuebijing protects against lipopolysaccharide-induced lung injury in rabbits. Exp Lung Res 2010;36(4):211–8.
[27] Gregoire M, Uhel F, Lesouhaitier M, et al. Impaired efferocytosis and neutrophil extracellular trap clearance by macrophages in ards. Eur Respir J 2018;52(2).
[28] Sayah DM, Mallavia B, Liu F, et al. Neutrophil extracellular traps are pathogenic in primary graft dysfunction after lung transplantation. Am J Respir Crit Care Med 2015;191(4):455–63.
[29] Okazaki M, Krupnick AS, Kornfeld CG, et al. A mouse model of orthotopic vascularized aerated lung transplantation. Am J Transplant 2007;7(6):1672–9.
[30] Gotzfried J, Smirnova NF, Morrone C, et al. Preservation with alpha1-antitrypsin improves primary graft function of murine lung transplants. J Heart Lung Transplant 2018;37(8):1021–8.
[31] Kanou T, Ohsumi A, Kim H, et al. Inhibition of regulated necrosis attenuates receptor-interacting protein kinase 1-mediated ischemia-reperfusion injury after lung transplantation. J Heart Lung Transplant 2018;37(10):1261–70.
[32] Wu Q, Gardiner GJ, Berry E, et al. ICOS-expressing lymphocytes promote resolution of CD8-mediated lung injury in a mouse model of lung rejection. PLoS ONE 2013;8(8):e72955.
[33] Martini T, Pavlisko EN, Chen DF, Palmer SM. Acute allograft rejection: cellular and humoral processes. Clin Chest Med 2011;32(2):295–310.
[34] Gregoire M, Tadie JM, Uhel F, et al. Frontline science: HMGB1 induces neutrophil dysfunction in experimental sepsis and in patients who survive septic shock. J Leukoc Biol 2017;101(6):1281–7.
[35] Robinson CA, Inci I, Naegeli M, et al. Extracorporeal photopheresis as second-line treatment therapy in life-threatening primary graft dysfunction following lung transplantation. Pediatr Transplant 2018;22(3):e13145.
[36] Liu Q, Wang J, Ma Y, Gu L. [A research on the influence of two herbal concoctions on toll-like receptor signal pathways of influenza virus induced pneumonia in mice]. Zhonghua Wei Zhong Bing Ji Jiu Yi Xue 2014;26(5):321–4.
[37] Gupta SK, Itagaki R, Zheng X, et al. miR-21 promotes fibrosis in an acute cardiac allograft transplantation model. Cardiovasc Res 2016;110(2):215–26.
[38] Glowacki F, Savary G, Gnemmi V, et al. Increased circulating miR-21 levels are associated with kidney fibrosis. PLoS ONE 2013;8(2):e58014.
[39] Liu G, Friggeri A, Yang Y, et al. miR-21 mediates fibrogenic activation of pulmonary fibroblasts and lung fibrosis. J Exp Med 2010;207(8):1589–97.
[40] Li H, Shi H, Gao M, et al. Long non-coding rna CASC2 improved acute lung injury by regulating miR-144-3p/AQP1 axis to reduce lung epithelial cell apoptosis. Cell Biosci 2018;8:15.
[41] Kong Q, Zhang S, Liang C, et al. LncRNA xist functions as a molecular sponge of miR-194-5p to regulate MAPK1 expression in hepatocellular carcinoma cell. J Cell Biochem 2018;119(6):4458–68.
[42] Tang Y, He R, An J, et al. lncRNA xist interacts with miR-140 to modulate lung cancer growth by targeting iASPP. Oncol Rep 2017;38(2):941–8.
[43] Schetter AJ, Nguyen GH, Bowman ED, et al. Association of inflammation-related and microRNA gene expression with cancer-specific mortality of colon adenocarcinoma. Clin Cancer Res 2009;15(18):5878–87.
[44] Aquino EN, Neves AC, Santos KC, et al. Proteomic analysis of neutrophil priming by paf. Protein Pept Lett 2016;23(2):142–51.
[45] Riyapa D, Buddhisa S, Korbsrisate S, et al. Neutrophil extracellular traps exhibit antibacterial activity against burkholderia pseudomallei and are influenced by bacterial and host factors. Infect Immun 2012;80(11):3921–9.
[46] Huang XL, Zhou XH, Zhou JL, et al. [Role of polymorphonuclear neutrophil in exogenous hydrogen sulfide attenuating endotoxin-induced acute lung injury]. Sheng Li Xue Bao 2009;61(4):356–60.
[47] Liu S, Su X, Pan P, et al. Neutrophil extracellular traps are indirectly triggered by lipopolysaccharide and contribute to acute lung injury. Sci Rep 2016;6:37252.
[48] Karpathakis A, Dibra H, Thirlwell C. Neuroendocrine tumours: cracking the epigenetic code. Endocr Relat Cancer 2013;20(3):R65–82.
[49] Hoffman SA, Wang L, Shah CV, et al. Plasma cytokines and chemokines in primary graft dysfunction post-lung transplantation. Am J Transplant 2009;9(2):389–96.
[50] Yang L, Wang B, Zhou Q, et al. MicroRNA-21 prevents excessive inflammation and cardiac dysfunction after myocardial infarction through targeting KBTBD7. Cell Death Dis 2018;9(7):769.
[51] Case SR, Martin RJ, Jiang D, et al. MicroRNA-21 inhibits toll-like receptor 2 agonist-induced lung inflammation in mice. Exp Lung Res 2011;37(8):500–8.
[52] Sun W, Ma M, Yu H, Yu H. Inhibition of lncRNA X inactivate-specific transcript ameliorates inflammatory pain by suppressing satellite glial cell activation and inflammation by acting as a sponge of miR-146a to inhibit NAV 1.7. J Cell Biochem 2018;119(12):9888–98.
[53] Zhao Y, Li S, Xia N, et al. Effects of XIST/miR-137 axis on neuropathic pain by targeting TNFAIP1 in a rat model. J Cell Physiol 2018;233(5):4307–16.